PCCP

PAPER

View Article Online
View Journal | View Issue

Cite this: *Phys. Chem. Chem. Phys.*, 2014, **16**, 21682

Raman mapping investigation of chemical vapor deposition-fabricated twisted bilayer graphene with irregular grains

Yuming Chen,†[a] Lijuan Meng,†[a] Weiwei Zhao,[b] Zheng Liang,[c] Xing Wu,[d] Haiyan Nan,[a] Zhangting Wu,[a] Shan Huang,[e] Litao Sun,[d] Jinlan Wang*[a] and Zhenhua Ni*[a]

Received 30th July 2014,
Accepted 22nd August 2014

DOI: 10.1039/c4cp03386h

www.rsc.org/pccp

Bilayer graphene as a prototype of two-dimensional stacked material has recently attracted great attention. The twist angle between graphene layers adds another dimension to control its properties. In this study, we used Raman mapping to investigate the twist angle dependence of properties of twisted bilayer graphene (TBG) with irregular grains that was fabricated by chemical vapor deposition (CVD). Different Raman parameters including intensity, width, and position of G and 2D peaks were used to distinguish TBG with different twist angles. The statistical results from Raman imaging on the distribution of twist angle are consistent with the results from selected area election diffraction (SAED). Finally, the Raman peak at approximately 1347 cm^{-1} for TBG with a large twist angle was assigned to the D-like peak, although it has similar excitation energy dependence of frequency as the defect-induced D peak. Theoretical calculation further confirmed that vacancy-like defect is not favored in the formation energy for TBG with a large twist angle as compared to monolayer graphene or TBG with other twist angles. These results will help to advance the understanding of TBG properties, especially for CVD samples with irregular grains.

Introduction

Twisted bilayer graphene (TBG) has recently attracted great attention, and many novel phenomena have been discovered such as the tunable energy difference between Van Hove Singularities (VHSs),[1] adjustable chirality tunneling,[2] and neutrino-like oscillation.[3] The twist angle is a crucial factor to determine the electronic and optical properties of TBG.[4–11] Bilayer graphene (BLG) fabricated by chemical vapor deposition (CVD) commonly contains a twist angle between graphene layers,[12–14] which has been viewed as a prototype to study the twist angle dependence of the interaction coupling in TBG.

Raman spectroscopy,[15–24] transmission electron microscopy (TEM),[12,22] and scanning tunneling microscopy (STM)[25] have been widely used to study the properties of TBG. Compared with other methods, Raman spectroscopy can provide sufficient information reflecting the electronic structure and phonon dispersion due to the strong electron–phonon interaction process involved. The intensity, full width at half maximum (FWHM), and position of the G and 2D peaks have been systematically studied as a function of the twist angle θ (θ = [0, 30°]), both experimentally and theoretically.[19,20] Raman mapping has also been used to study the twist angle dependence of the G peak resonance of TBG.[15,18] Furthermore, extra peaks including R,[16] R′,[17] and D-like[16] peaks in TBG, which are absent in monolayer graphene, reveal its unique characteristics. Partially grown CVD graphene with a regular hexagonal shape assists with the identification of the twist angle, and therefore, is frequently adopted in Raman studies.[14,22,26]

In our work, Raman mapping is used as an efficient way to distinguish the twist angles of TBG prepared by CVD with irregular grains or joint grains, which has lost its original morphology during the grain-merging process. The TBG samples are classified into three types according to the twist angle, and can be clearly distinguished using Raman mapping with different parameters, *e.g.*, I_G, I_{2D}, and $FWHM_{2D}$. The statistical results of twist angles from SAED are consistent with the Raman mapping results, which indicates the preferential growth of AB-stacked

[a] *Department of Physics, Southeast University, Nanjing 211189, China. E-mail: zhni@seu.edu.cn, jlwang@seu.edu.cn*
[b] *Jiangsu Key Laboratory for Design and Fabrication of Micro-Nano Biomedical Instruments, School of Mechanical Engineering, Southeast University, Nanjing 211189, China*
[c] *Graphene Research and Characterization Center, Taizhou Sunano New Energy Co., Ltd., Taizhou 225300, China*
[d] *SEU-FEI Nano-Pico Center, Key Laboratory of MEMS of the Ministry of Education, School of Electrical Science and Engineering, Southeast University, Nanjing 210096, China*
[e] *School of Material Science and Engineering, Southeast University, Nanjing 211189, China*
† These authors contributed equally.

BLG and 30° TBG. Moreover, it reveals a D-like peak that is frequently observed in TBG but sometimes is assigned to the defect-induced D peak.[14,19]

Experimental

Sample preparation

Bilayer graphene was synthesized using low-pressure CVD on a copper foil (thickness of 25 μm, 99.9% purity). The flux of hydrogen was maintained at 96 sccm during the entire heating process, and 6 sccm methane (CH_4) was introduced at the growth temperature of 1045 °C and maintained for 90 min. After growth, the graphene sample was transferred onto a SiO_2 (300 nm)/Si substrate for optical and Raman characterization or onto a copper grid for TEM analysis using a standard PMMA transfer process.[27]

Raman and TEM measurements

The Witec 300R confocal Raman system was used to obtain the Raman spectra and mappings. The excitation laser was tuned to wavelengths of 532 nm (2.33 eV) and 633 nm (1.96 eV), and the laser power was kept below 1 mW to avoid laser-induced sample heating or damage. The Raman mapping was acquired by a 100× objective using a 532 nm laser with a spot size of approximately 300 nm. The Witec Project 2.10 software was used for data analysis, creating a histogram of the integrated intensity, and achieving the Raman mapping. The SAED results were carried out with a Tecnai G2 T20 TEM with a voltage of 200 kV.

Density functional theory calculations

The density functional theory (DFT) calculations were implemented using the Vienna ab initio Simulation Package (VASP).[28,29] The ion–electron interactions were described by the projected augmented wave (PAW) method.[30] The exchange correlation energy was described in the generalized gradient approximation (GGA) using the PBE functional including van der Waals corrections (DFT-D2 Grimme's method).[31] All the structures were optimized until the force acting on each atom was less than 0.02 eV $Å^{-1}$. The kinetic energy cutoff was chosen as 400 eV. The Brillouin zone was sampled by 7 × 7 × 1 to 1 × 1 × 1 grid meshes using the Monkhorst–Pack scheme and varied from the smallest to larger unit cell calculations.

A TBG was built according to the method from ref. 32. In a hexagonal lattice whose cell basis vector is $\boldsymbol{a}$ and $\boldsymbol{b}$, a supercell basis vector can be constructed as $n\boldsymbol{a} + m\boldsymbol{b}$, where n and m are integers. The corresponding angle of the supercell basis vector relative to the zigzag direction can be derived as $\varphi = \cos^{-1}\left(\frac{n+m/2}{\sqrt{n^2+nm+m^2}}\right)$. For bilayer graphene, we denote the first layer supercell basis vector as $n_1\boldsymbol{a} + m_1\boldsymbol{b}$ and the second as $n_2\boldsymbol{a} + m_2\boldsymbol{b}$. We look for a set of integers to make the magnitude of supercell basis vectors of two layers match or approximately match. Thus, the twist angle between bilayer graphene is $\theta = \varphi_1 - \varphi_2$. For those mismatched supercells, we choose the smallest supercell for which the strain is less than 1%.

The formation energy of a single vacancy in TBG is defined according to the following equation:

$$E_{\text{vacancy}} = E_{\theta+\text{vacancy}} + E_{\text{C}} - E_{\theta} \quad (1)$$

where $E_{\theta+\text{vacancy}}$ and E_{θ} are the energies of TBG with and without a single atom vacancy; E_{C} is the energy of one carbon atom in TBG.

Results and discussion

The optical image of a TBG sample with irregular grains is shown in Fig. 1(a). The growth mechanism of CVD multilayer graphene on a copper substrate has been previously studied.[33] Fig. 1(b) is the Raman mapping of the integrated intensity of G peak, which is the first-order Raman peak with phonon vector

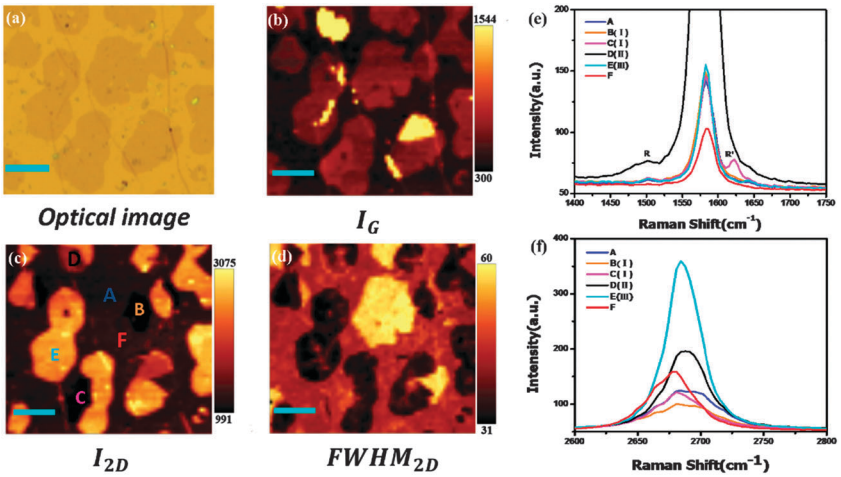

Fig. 1 (a) Optical image of CVD graphene film containing irregular bilayer grains. Raman imaging of the G peak intensity (b), 2D peak intensity (c), and 2D peak FWHM (d) of the same sample; all the scale bars are 7 μm. The G peak (e) and the 2D peak (f) Raman spectra correspond to points A–F in (c). Point F refers to monolayer graphene.

$q = 0$ to fulfill the momentum conservation. The Raman mapping can be divided into two parts – monolayer domains, and bilayer domains, which are nearly twice the G peak intensity. Note that some of the bilayer domains have a G peak intensity tens of times that of monolayer graphene, which corresponds to TBG with the G peak resonance at a particular twist angle.[18,19] The striking enhancement of the G peak can be seen from the single spectrum in Fig. 1(e) as well. The critical condition for G resonance is that the difference between the conduction and valence VHSs of TBG approximately matches the laser energy.[19] The critical G resonance angle θ_C obeys the following equation:[19]

$$\theta_C = 3aE_{laser}/\hbar V_f 4\pi \quad (2)$$

where a is the lattice parameter (2.46 Å), $\hbar$ is the reduced Planck's constant and V_f is the Fermi velocity in single layer graphene (approximately 1.0×10^6 m s^{-1}). According to the equation, the G resonance occurs at a twist angle of approximately 12° for E_{laser} = 2.33 eV (532 nm) for TBG.

The twist angle can be classified according to the interlayer coupling. It has been proven experimentally and theoretically that a drastic decrease of Fermi velocity and obvious electron–hole asymmetry can be observed for TBG with small angles ($\theta < 8°$), resulting from the strong interlayer coupling.[6,34,35] Remarkably, the Fermi velocity approximates to zero for angles $\theta < 3°$, which is related to the localization of Dirac electrons on account of the adjacent VHSs.[6,34] For a twist angle larger than 20°, TBG shows almost indistinguishable electronic properties from monolayer graphene, where the large energy difference from the VHSs to the Fermi level indicates that two graphene layers almost decouple.[6] The intermediate angle ($8° < \theta < 20°$) is a transition state of the strong and weak interlayer coupling of TBG. Accordingly, the TBG samples could be classified into three types, namely small angle (I, $\theta < 8°$), intermediate angle (II, $8° < \theta < 20°$), and large angle (III, $\theta > 20°$). It should be noted that the exact transition angle between different types could be slightly different due to the experimental uncertainty.

Previous results have shown that I_{2D} is closely related to the twist angle and the strength of interlayer coupling, *i.e.*, I_{2D} increases with the increase of the twist angle.[19,20] Consequently, I_{2D} is advantageous in the classification of twist angles. In the Raman imaging of I_{2D} (Fig. 1(c)), the small angle (I, $\theta < 8°$) corresponds to points B and C, whose intensities are weaker than that of AB-stacked BLG. Notably, the Raman signals of points B and C also show differences. The I_{2D} of point B is slightly weaker than that of point C, but the $FWHM_{2D}$ is much larger, as shown in Fig. 1(d), with a magnitude of 60 cm^{-1} and 45 cm^{-1} for points B and C, respectively. In addition, a new Raman mode named R′ (approximately 1625 cm^{-1}) appears in point C, which originates from an intravalley process with the interaction of electrons, LO phonons, and interior folded phonons.[17] The R′ peak can be observed in TBG with a twist angle from 3–8° for visible excitations as previously reported.[22] Therefore, point B lies in the region of $\theta < 3°$, while point C lies in the region of $3° < \theta < 8°$. Theoretical calculations also predicted the similar trend of intensity and width of the 2D peak in the small angle region.[20]

Within the intermediate angle (II, $8° < \theta < 20°$) scope, the I_{2D} increases monotonously with the increase in the twist angle. Point D in Fig. 1(c) belongs to the intermediate angle, and this point has a striking enhancement of I_G, nearly 20 times stronger than that of monolayer graphene as shown in Fig. 1(b) and (e).

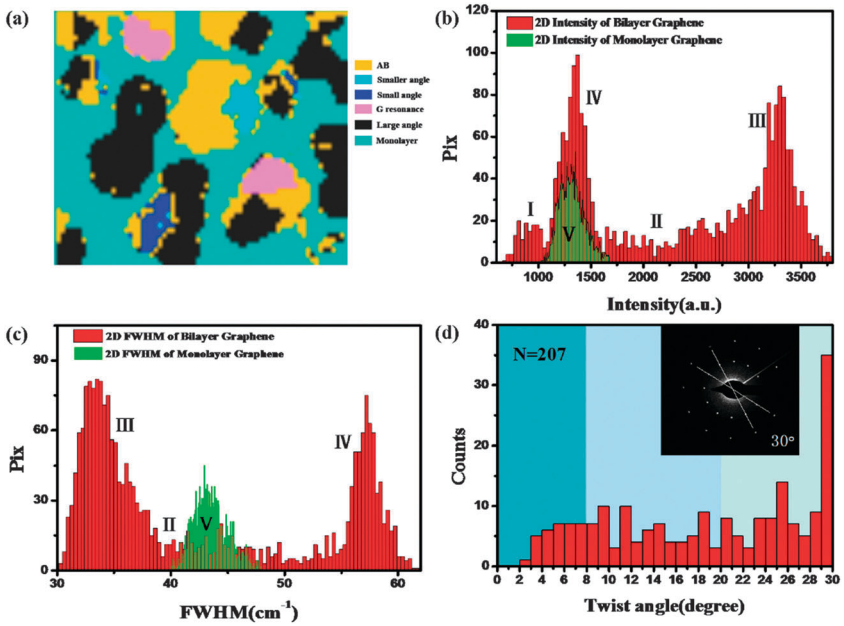

Fig. 2 (a) The distribution of various twist angles corresponds to the area in Fig. 1(a), which is filled with false colors. (b) and (c) The pix distribution of the 2D peak integrated intensity and FWHM of monolayer and bilayer graphene. (d) The statistical distribution of twist angles of 207 CVD TBG samples; the insert is a typical SAED pattern of 30° TBG.

Accompanying the G peak resonance, another double resonant Raman mode called R peak is observed, as shown in Fig. 1(e).[17,23] To complete this double resonance process, an intervalley process including TO phonon and folded phonon scattering is proposed.[17] It should be noted that the G resonance and R peak will only be observed for angles that fulfill the resonant condition (eqn (2), approximately 12° for 532 nm excitation in our work). They can even be observed in the large angle region (III) with very large excitation energy (*e.g.*, deep UV).[24] When the twist angle reaches the large angle range (III, $\theta > 20^\circ$), the I_{2D} saturates at 2–3 times that of monolayer graphene.[19,20] The $FWHM_{2D}$ of TBG with a large angle is close to monolayer graphene (approximately 33 cm^{-1}) because the two graphene layers almost decouple. Large regions in Fig. 1(c) belong to the large angle type (III), *e.g.*, point E.

Based on the above classification, regions with different types of angles are unambiguously extracted and shown by different colors in Fig. 2(a). Fig. 2(b) gives the histogram of I_{2D} of the same sample, and it corresponds to five types of samples, including I (small angle), II (intermediate angle), III (large angle), IV (AB stacked) and V (single layer). The histogram of corresponding $FWHM_{2D}$ is marked using the same notations (Fig. 2(c)). As shown in Fig. 2(b) and (c), each type of twist angle occupies a single peak except angles with small components such as the intermediate angle (II). To further explore the angle distribution, 207 TBG samples were studied by TEM, and the statistical results of twist angles are displayed in Fig. 2(d). It was found that the largest quantity of twist angles in TBG were those with an angle of approximately 30°, and its typical diffraction pattern is shown in the insert of Fig. 2(d). This indicates that the formation of 30° TBG is more preferential during the CVD growth process. It is proposed that the strong interaction between the graphene edge and the catalytic substrate[36] or the copper foil[26] contribute to the orientational growth of multilayer graphene, *i.e.*, AB stacked and 30° TBG. However, the proportion of the approximately 30° TBG in Fig. 2 is comparatively lower than that in ref. 26, because factors such as the growth rate or the surface roughness of the copper foil may influence the orientation of the nucleus.

The TBG sample in Fig. 3 can also be easily identified as AB stacked (region 2) and large angle (region 1). Fig. 3(c) and (e) clearly show a peak located at approximately 1347 cm^{-1} for TBG with a large angle, while other types of TBG and monolayer graphene do not contain such a peak. Fig. 3(f) shows that this particular peak has the same position as the defect-induced D peak in monolayer graphene collected from the edges.[37] Moreover, the frequency of this peak presents linear dispersion with excitation laser energy, and the slope is approximately 47 cm^{-1} eV^{-1} as presented in the inset of Fig. 3(f), which is comparable with the value of the D peak.[38] Similar phenomena have also been observed in folded graphene (or TBG) by mechanical cleavage that does not contain noticeable defects, and this particular structure was assigned to a D-like peak originating from the Fourier components of periodical potential.[16] Therefore, the question is whether this peak in the CVD TBG sample is related to defects, such as vacancies or grain boundaries in the graphene lattice (D peak), or due to the intrinsic natures of TBG with a large angle (D-like peak).

The formation energies ($E_{vacancy}$) of a single vacancy in TBG with different angles are calculated and displayed in Fig. 4, which provides information on the formation of vacancies in the growth of TBG. Here, we only consider the vacancy-like defect, as grain boundaries[39] cannot contribute to the uniform distribution of the approximately 1347 cm^{-1} peak as shown in Fig. 3(c). Fig. 4(a) and (b) present the optimized structures of TBG with 0° and 30° twist angles, with a single vacancy labeled by red circles. As shown in Fig. 4(c), AB-stacked BLG possesses the largest $E_{vacancy}$ (approximately 8.0 eV), which indicates that vacancies are least likely to be formed. The $E_{vacancy}$ of TBG with

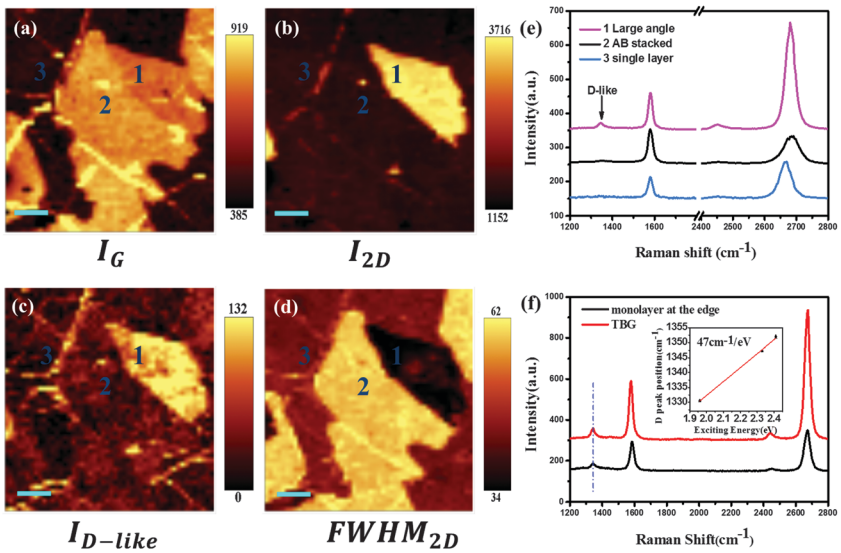

Fig. 3 Raman imaging of the G peak intensity (a), 2D peak intensity (b), D-like peak intensity (c), and 2D peak FWHM (d) of a CVD graphene with irregular TBG grains; all the scale bars are 4 μm. (e) Raman spectra correspond to the regions labeled 1, 2, and 3 in (d). (f) Raman spectra of TBG with large angle and monolayer graphene edges (with a defect-induced D peak). The insert reflects the dispersion of peak position as a function of the excitation energy.

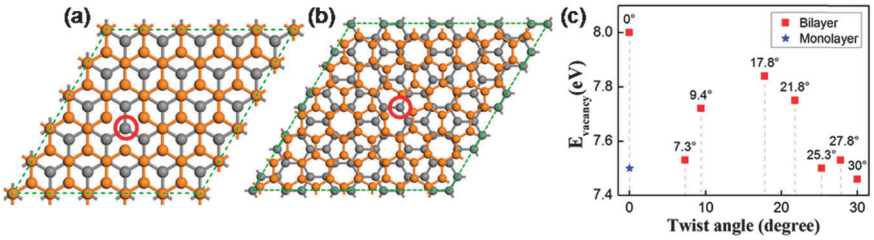

Fig. 4 The calculation of the vacancy formation energy of TBG: (a) and (b) typical bilayer lattice structures with 0° and 30° twist angles, respectively; the vacancy locations are denoted with red circles. (c) The DFT results of $E_{vacancy}$ with various twist angles. The blue star represents the $E_{vacancy}$ of monolayer graphene reported in ref. 40.

θ = 7.3° is approximately 7.53 eV, which is nearly the same as that of the large angle type (approximately 7.46 eV for θ = 30°). Moreover, the formation energy of a single vacancy in monolayer graphene reported in ref. 40 is approximately 7.5 eV,[40] which is also comparable to that of large angles in our calculation. As a consequence, the formation of vacancy is not energetically favored for TBG with a large angle, and therefore, the 1347 cm^{-1} peak in TBG with a large angle should be a D-like peak due to the scattering of periodical potential of the TBG lattice,[16] but not a defect-related peak.

Conclusions

We have shown that Raman mapping analysis could provide fruitful information regarding CVD TBG samples. The G peak Raman intensity image helps to distinguish G resonance regions (with a twist angle of approximately 12° for excitation energy of 2.33 eV) from other types of bilayer structures as well as monolayer, while three types of twist angles, namely small, intermediate and large angles, could be distinguished in the 2D peak intensity/FWHM images. It was also revealed that TBG with a large angle presents a D-like peak due to elastic scattering of static periodic potential, whose frequency is laser energy-dependent (similar to D peak). The calculated single vacancy formation energy of a monolayer and TBG with different twist angles further confirms that this peak is not related to the lattice defect in TBG, as it is not favored in the formation energy. The Raman mapping results provide an easy, convenient, and nondestructive way to study the twist angle-dependent properties of CVD TBG, which could also assist with future studies of two-dimensional materials and heterostructures.

Acknowledgements

This work was supported by the NSFC (11104026, 61422503, 61376104, 21173040, 21373045), the Program for New Century Excellent Talents in University (NCET-11-0094), the NBRP (2010CB923401, 2011CB302004), the Natural Science Foundation of Jiangsu Province (BK2011585, BK20130016), the SRFDP (20130092110029), and the Open Research Fund of the SEU-JGRI Joint Research Center of Advanced Carbon Materials, as well as the State Key Laboratory of Advanced Optical Communication Systems and Networks.

References

1 G. H. Li, A. Luican, J. Dos Santos, A. Neto, A. Reina, J. Kong and E. Y. Andrei, *Nat. Phys.*, 2010, **6**, 109.
2 W. Y. He, Z. D. Chu and L. He, *Phys. Rev. Lett.*, 2013, **111**, 066803.
3 L. D. Xian, Z. F. Wang and M. Y. Chou, *Nano Lett.*, 2013, **13**, 5159.
4 Y. Y. Wang, Z. H. Ni, L. Liu, Y. H. Liu, C. X. Cong, T. Yu, X. J. Wang, D. Z. Shen and Z. X. Shen, *ACS Nano*, 2010, **4**, 4074.
5 M. Y. Choi, Y. H. Hyun and Y. Kim, *Phys. Rev. B: Condens. Matter Mater. Phys.*, 2011, **84**, 195437.
6 A. Luican, G. H. Li, A. Reina, J. Kong, R. R. Nair, K. S. Novoselov, A. K. Geim and E. Y. Andrei, *Phys. Rev. Lett.*, 2011, **106**, 126802.
7 W. Yan, M. X. Liu, R. F. Dou, L. Meng, L. Feng, Z. D. Chu, Y. F. Zhang, Z. F. Liu, J. C. Nie and L. He, *Phys. Rev. Lett.*, 2012, **109**, 126801.
8 K. S. Kim, A. L. Walter, L. Moreschini, T. Seyller, K. Horn, E. Rotenberg and A. Bostwick, *Nat. Phys.*, 2013, **12**, 887.
9 P. Moon and M. Koshino, *Phys. Rev. B: Condens. Matter Mater. Phys.*, 2013, **87**, 205404.
10 P. Hofmann, *Nat. Mater.*, 2013, **12**, 874.
11 R. W. Havener, Y. Liang, L. Brown, L. Yang and J. Park, *Nano Lett.*, 2014, **14**, 3353.
12 L. Brown, R. Hovden, P. Huang, M. Wojcik, D. A. Muller and J. Park, *Nano Lett.*, 2012, **12**, 1609.
13 J. Campos-Delgado, G. Algara-Siller, C. N. Santos, U. Kaiser and J. P. Raskin, *Small*, 2013, **9**, 3247.
14 S. R. Xing, W. Wu, Y. A. Wang, J. M. Bao and S. S. Pei, *Chem. Phys. Lett.*, 2013, **580**, 62.
15 Z. H. Ni, L. Liu, Y. Y. Wang, Z. Zheng, L. J. Li, T. Yu and Z. X. Shen, *Phys. Rev. B: Condens. Matter Mater. Phys.*, 2009, **80**, 125404.
16 A. K. Gupta, Y. J. Tang, V. H. Crespi and P. C. Eklund, *Phys. Rev. B: Condens. Matter Mater. Phys.*, 2010, **82**, 241406.
17 V. Carozo, C. M. Almeida, E. Ferreira, L. G. Cancado, C. A. Achete and A. Jorio, *Nano Lett.*, 2011, **11**, 4527.
18 R. W. Havener, H. L. Zhuang, L. Brown, R. G. Hennig and J. Park, *Nano Lett.*, 2012, **12**, 3162.
19 K. Kim, S. Coh, L. Z. Tan, W. Regan, J. M. Yuk, E. Chatterjee, M. F. Crommie, M. L. Cohen, S. G. Louie and A. Zettl, *Phys. Rev. Lett.*, 2012, **108**, 246103.

20 S. Coh, L. Z. Tan, S. G. Louie and M. L. Cohen, *Phys. Rev. B: Condens. Matter Mater. Phys.*, 2013, **88**, 165431.
21 A. Jorio and L. G. Cancado, *Solid State Commun.*, 2013, **175**, 3.
22 C. C. Lu, Y. C. Lin, Z. Liu, C. H. Yeh, K. Suenaga and P. W. Chiu, *ACS Nano*, 2013, **7**, 2587.
23 V. Carozo, C. M. Almeida, B. Fragneaud, P. M. Bede, M. Moutinho, J. Ribeiro-Soares, N. F. Andrade, A. G. Souza, M. Matos, B. Wang, M. Terrones, R. B. Capaz, A. Jorio, C. A. Achete and L. G. Cancado, *Phys. Rev. B: Condens. Matter Mater. Phys.*, 2013, **88**, 085401.
24 Y. N. Wang, Z. H. Su, W. Wu, S. Nie, N. Xie, H. Q. Gong, Y. Guo, J. H. Lee, S. R. Xing, X. X. Lu, H. Y. Wang, X. H. Lu, K. McCarty, S. S. Pei, F. Robles-Hernandez, V. G. Hadjiev and J. M. Bao, *Appl. Phys. Lett.*, 2013, **103**, 123101.
25 I. Brihuega, P. Mallet, H. Gonzalez-Herrero, G. T. de Laissardiere, M. M. Ugeda, L. Magaud, J. M. Gomez-Rodriguez, F. Yndurain and J. Y. Veuillen, *Phys. Rev. Lett.*, 2012, **109**, 196802.
26 Z. Yan, Y. Y. Liu, L. Ju, Z. W. Peng, J. Lin, G. Wang, H. Q. Zhou, C. S. Xiang, E. Samuel, C. Kittrell, V. I. Artyukhov, F. Wang, B. I. Yakobson and J. M. Tour, *Angew. Chem., Int. Ed.*, 2014, **53**, 1565.
27 J. Kang, D. Shin, S. Bae and B. H. Hong, *Nanoscale*, 2012, **4**, 5527.
28 G. Kresse and D. Joubert, *Phys. Rev. B: Condens. Matter Mater. Phys.*, 1999, **59**, 1758.
29 G. Kresse and J. Furthmuller, *Comput. Mater. Sci.*, 1996, **6**, 15.
30 P. E. Blochl, *Phys. Rev. B: Condens. Matter Mater. Phys.*, 1994, **50**, 17953.
31 S. Grimme, *J. Comput. Chem.*, 2006, **27**, 1787.
32 H. P. Komsa and A. V. Krasheninnikov, *Phys. Rev. B: Condens. Matter Mater. Phys.*, 2013, **88**, 085318.
33 Q. Y. Li, H. Chou, J. H. Zhong, J. Y. Liu, A. Dolocan, J. Y. Zhang, Y. H. Zhou, R. S. Ruoff, S. S. Chen and W. W. Cai, *Nano Lett.*, 2013, **13**, 486.
34 G. Trambly De Laissardiere, D. Mayou and L. Magaud, *Nano Lett.*, 2010, **10**, 804.
35 J. Dos Santos, N. Peres and A. H. Castro, *Phys. Rev. Lett.*, 2007, **99**, 256802.
36 X. Y. Zhang, Z. W. Xu, L. Hui, J. Xin and F. Ding, *J. Phys. Chem. Lett.*, 2012, **3**, 2822.
37 Y. N. Xu, D. Zhan, L. Liu, H. Suo, Z. H. Ni, T. N. Thuong, C. Zhao and Z. X. Shen, *ACS Nano*, 2011, **5**, 147.
38 I. Pocsik, M. Hundhausen, M. Koos and L. Ley, *J. Non-Cryst. Solids*, 1998, **227**, 1083.
39 J. F. Zhang and J. J. Zhao, *J. Appl. Phys.*, 2013, **113**, 043514.
40 F. Banhart, J. Kotakoski and A. V. Krasheninnikov, *ACS Nano*, 2011, **5**, 26.